# Influence of spatial delay on the modulational instability in a composite system with a controllable nonlinearity

Monisha Kumar,[1] K. Nithyanandan,[2,3] and K. Porsezian[1,*]

[1]*Department of Physics, School of Physical, Chemical and Applied Sciences, Pondicherry University, Pondicherry 605014, India*

[2]*Laboratoire Interdisciplinaire Carnot de Bourgogne, UMR 6303 CNRS, Université de Bourgogne, 9 avenue A. Savary, BP 47870, Dijon Cedex F-21078, France*

[3]*CNRS/Universite Joseph Fourier, Laboratoire Interdisciplinaire de Physique (LIPHY), F-38400 Grenoble, France*

(Received 15 December 2017; published 18 June 2018)

A theoretical investigation of the modulational instability (MI) in a composite system with a nonlocal response function is presented. A composite system of silver nanoparticles in acetone is chosen, whose nonlinearity can be delicately varied by controlling the volume fraction of the constituents, thus enabling the possibility of nonlinearity management. A pump-probe counterpropagation configuration has been assumed, and the interplay between the competing nonlinearities and the nonlocalities in the MI dynamics is systematically explored. A different class of nonlocalities have been considered, and the study reveals that the nonlocality critically depends on the kind of nonlocal function. However, the general behavior is that the strength of nonlocality suppresses the MI gain, while for a rectangular function it assists the emergence of new spectral windows. We also show that the cross coupling effects are significant in enhancing MI, especially in the defocusing nonlinearity. We also emphasize the impact of the relative strength of the nonlinearities in the MI dynamics at different settings of competing nonlinearities. Thus, we emphasize the importance of the different class of nonlocal response in the MI dynamics and explore the interplay between the higher order nonlinear effects and nonlocalities in the counterpropagating configurations.

DOI: 10.1103/PhysRevE.97.062208

## I. INTRODUCTION

Advancements in material chemistry and photonic technologies have opened new frontiers in research on plasmonics and nanophotonics. Of late, particularly, "composites" with interesting controllable physical properties played a vital role in the development of novel plasmonic applications. A composite is a material made from two or more constituent materials with distinct physical and chemical properties, that when combined produce a material with different characteristics from individual components. Commonly used composites are of two types: (1) spatially separated metal nanoparticles embedded in a dielectric host and (2) fractal aggregates of metal nanoparticles [1]. For systems containing a metallic nanoparticle, the surface plasmon resonance (SPR) plays an important role, modifying, for instance, linear and nonlinear optical properties of the material [2,3].

In the development of the novel materials aiming at photonic applications, colloidal systems containing metal nanoparticles are very promising owing to the enhancements of the nonlinear absorption and nonlinear refractive index observed in such systems [4,5]. These changes in the nonlinear optical properties of a colloid can be mainly attributed to two different origins: a local field effect and large nonlinear response of metals. Thermal properties of metal nanocomposites critically depend on the concentration of nanoparticles and play an important role in the determination of the colloid characteristics of the composite structure. For example, it was found in a colloidal system of gold nanoparticles in castor oil, that, even though the laser wavelength was not resonant with the surface plasmon absorption band, significant enhancement of electronic and thermal nonlinearities was observed. The presence of nanoparticles enhanced both local (electronic) and nonlocal (thermal) nonlinear response of the colloids. The electronic part of the nonlinearity was enhanced by at least two orders of magnitude depending on the particle-filling fraction. On the other hand the thermo-optical properties of the colloidal systems is rather more sensitive and changes dramatically as the filling fraction was increased [6].

During the last century or so, optical properties of nanoparticles have been extensively studied, and metal-dielectric nanocomposites (MDNCs) have found various applications in different fields of science and technology. Since the optical properties of metal nanoparticles are typically governed by SPR, they are strongly dependent on the nanoparticles size, shape, concentration, and spatial distribution as well as on the properties of the surrounding matrix. Control over these parameters enables such MDNCs to become promising media for the development of novel nonlinear materials, nanodevices, and optical elements [7]. Especially, in the context of nonlinear plasmonics, the MDNCs are promising contenders and play an indispensable role in realizing a system endowed with nonlinearity management [8]. The emergence of nonlinear plasmonics has developed a renewed interest in the studies related to higher-order nonlinearities (HONs). MDNCs happened to be an ideal candidate to serve the purpose of delicate management of nonlinearity by an appropriate ratio of the volume fraction of nanoparticles to that of the host. This way of controlling the nonlinearity of the system is advantageous

*ponzsol@gmail.com

 ©2018 American Physical Society

indeed, as it would enable "on demand" control on each order of nonlinear susceptibility in the system. For instance, by a proper choice of the volume fraction of nanoparticles, one can even nullify the cubic nonlinearity while the quintic or septimal nonlinearities can still be finite [9]. This enables one to tailor-make the effective nonlinearity, making MDNCs potential choices for nonlinear management. In the recent past, competing nonlinearities also have drawn much attention. Such nonlinearities occur in media where a few different physical processes contribute to the overall nonlinear response. A few examples to mention are Bose-Einstein condensates with simultaneous local and long-range interactions [10] and nematic liquid crystals with comparable thermal and orientational nonlinearities [11].

Another interesting feature typical to the systems like MDNCs is the nonlocal nonlinearity, meaning that the nonlinearity is a nonlocal function of the incident field. Even though there are a lot of studies on nonlocal nonlinearities in the soliton context, most of them are related to the studies on propagation in the fibers and BECs [11–13]. For instance, in the case of single dark spatial solitons, nonlocality tends to expand the width of the solitons. Spatial nonlocality provides stabilization of bright solitons and induces their attraction, even if they are out of phase, and in the case of dark solitons, attraction induced by nonlocality can lead to the formation of their band states, and in the case of vortices nonlocality can stabilize the vortex propagation [14].

One of the intriguing manifestations in the propagation dynamics of any nonlinear media is the so-called modulation instability (MI). MI is a nonlinear phenomenon, where a continuous wave (CW) or a quasi-CW undergoes a modulation of its amplitude or phase in the presence of noise or any other weak perturbations. The modulation process may eventually grow and lead to the breakdown of the wave into a train of short pulses or filaments. The phenomenon of MI has been studied in a wide variety of physical systems like fluid dynamics [15,16], plasma physics [17,18], nonlinear fiber optics [19], Bose-Einstein condensates [20–22], liquid crystals [23–25], and various plasmonic systems [26–28]. It has been shown that MI is strongly affected by various mechanisms in the nonlinear system [29–32], and in particular, the nonlocality in nonlinear response [33,34] is another intriguing effect that plays a substantial role in the dynamics of the system.

Recently Reyna *et al.* reported an experimental study on a composite system made up of silver nanoparticles suspended in acetone. In this important work, the authors successfully realized a composite system with flexible nonlinearity management where the effective Kerr nonlinearity can be controlled at will, by merely changing the volume fraction of the silver nanoparticles. In this way, they demonstrated different aspects of nonlinearity management, and one interesting case would be the zero cubic nonlinearity with finite quintic nonlinearity. Indeed, this particular case is interesting, as it is not possible in the conventional system. In a similar context, they also studied the dynamics of spatial MI at different settings in the limit of effective local nonlinear response. In principle, in composite systems as in Ref. [35], the nonlinearity is not strictly local, and the effective nonlinearity is a nonlocal function of the incident field. This is particularly true because of the strong confinement of electric field due to the formation of plasmonic modes in metal nanoparticles, which can enhance the nonlinear effects whose strength crucially depends on the particular function of nonlocality. Therefore in order to accurately model the dynamics, one has to incorporate the nonlocality in the nonlinear response. Of late, there had been a few studies on MI in nonlocal nonlinear media. To mention a few, Krolikowski *et al.* studied MI in nonlocal nonlinear Kerr media with different kinds of nonlocalities like weak, strong, and general nonlocal effects [36]. Wang *et al.* studied MI in nonlocal Kerr media with sine-oscillatory response [37]. Tiofack *et al.* studied the effect of competing cubic-quintic nonlinearities on MI in non-Kerr-type media showing equal nonlocal response functions [38], and MI in media with a local quintic and nonlocal cubic nonlinearities was studied in Ref. [39].

Most cases of nonlocal MI studies are primarily based on single optical beam, and such a kind of MI is termed a scalar MI. The copropagation(or counterpropagation) of two or more optical beams can lead to interesting and peculiar phenomena which could not be realized in the single-beam case [40,41]. In fact, one of the breakthroughs in MI is the realization of MI in normal dispersion (or diffraction) regime [40]. As is known the normal group velocity dispersion (GVD) regime is not subject to the MI process, due to the lack of phase matching between the dispersion and nonlinear components of the system. But the nonlinear coupling between the two copropagating beams due to the cross-phase modulation (XPM) (i.e., refractive index seen by one wave depends on the intensity of the copropagating wave through the XPM coefficient) destabilizes the steady state, leading to frequency modulation even in the normal GVD regime [40,41]. These interesting results set the benchmark for the extensive work on two-color light propagation in the optical system.

Motivated by the interesting nonlinear properties associated with the composite structure, and the physical importance of a coupled nonlinear system in the MI process, in what follows, we study the XPM-induced spatial MI in a composite system with a nonlocal nonlinear response. Taking the advantage of the recent experimentally realized composite system made up of silver nanoparticles suspended in acetone by Reyna *et al.*, our study focuses on the coupled system in the same settings, with particular emphasis on the different functional forms of nonlinear responses. The paper is organized as follows: Sec. II describes the theoretical model and the propagation equation. In Sec. III we have applied linear stability analysis followed by the study of modulation instability with various nonlocal response functions for different competing nonlinearities in Sec. IV. Section V gives the conclusions.

## II. THEORETICAL MODEL

The counterpropagation of pump-probe beams in the composite medium is governed by the modified coupled nonlinear Schrödinger equation of the form

$$(-1)^j i\frac{\partial A_j}{\partial \xi}+\frac{1}{2}\frac{\partial^2 A_j}{\partial \rho^2}+\alpha_1\left(|A_j|^2+2|A_{3-j}|^2\right)A_j +\alpha_2\left(|A_j|^4+6|A_j|^2|A_{3-j}|^2+3|A_{3-j}|^4\right)A_j=0, \quad (1)$$

where $A_j$ with $j = 1,2$ the amplitude of the pump and probe beams in the composite medium, respectively. Here the spatial coordinates have been normalized to $K^{-1} = \frac{\lambda}{2\pi n_0}$, where $n_0$ is the linear refractive index of the host medium and $\lambda$ is the wavelength of the laser pump. $\xi$ is the dimensionless direction of propagation, which is defined as $\xi = zK$ and the dimensionless transverse coordinate $\rho$ is given by $\rho = xK$. $\alpha_1$ and $\alpha_2$ are the strengths of the competing cubic and quintic nonlinearities, respectively, and it takes a positive (negative) sign for self-focusing (defocusing) nonlinearities.

Reyna *et al.* proposed this model for light propagation in MDNC and studied the nonlinearity management and spatial modulation instability for cubic quintic nonlinearity [35], the two-dimensional solitons for a quintic septimal medium [9], and the spatial phase modulation in the medium with quintic septic nonlinearity [42]. The theoretical model was developed using the generalized Maxwell-Garnet model under the assumption of a homogenous, isotropic medium with the nanoparticles uniformly distributed. The particle size $a$ is smaller than the interparticle distance $b$, which is smaller than the incident light wavelength $\lambda$.

Spatial nonlocality comes into the picture when the nonlinear refractive index at a given point is determined not only by the light intensity at that point but also by the intensity near that point. A phenomenological generic form of nonlocal nonlinear response induced by an optical beam of intensity $I(\rho,\xi)$ [36] is given by

$$\Delta n(I) = S\int_{-\infty}^{\infty} R(\rho-\rho')I(\rho',\xi)\,d\rho', \tag{2}$$

where $\Delta n(I)$ is the intensity-dependent change in the refractive index of the medium, and the right-hand side gives a spatial convolution integral with $R(\rho)$ as the nonlocal response function defining the nonlocal character of the nonlinearity and its width (compared to the spatial extent of the beam) determines the degree of nonlocality with $S$ representing the strength and sign of the nonlinear contribution. In the limiting case of $R(\rho) = \delta(\rho)$ Eq. (2) describes the local response [38,43,44]. Even though the nonlocality model mentioned by Eq. (2) is phenomenological, it very well describes the features of nonlocal media. Typical nonlocal systems involve media with transport processes such as ballistic atomic transport or heat diffusion as in atomic vapors or charge transport in photorefractive crystals or charge separation in thermal media or plasma. Also long-range interactions are responsible for nonlocal responses in liquid crystals or dipolar BECs [14,45].

The coupled NLSE with the phenomenological generic model of competing nonlocal nonlinear responses is given by [35,38]

$$\begin{aligned}(-1)^j i\frac{\partial A_j}{\partial\xi} + \frac{1}{2}\frac{\partial^2 A_j}{\partial\rho^2} + \alpha_1\int_{-\infty}^{\infty} R_1(\rho-\rho')(|A_j|^2 \\ + 2|A_{3-j}|^2)A_j\,d\rho' + \alpha_2\int_{-\infty}^{\infty} R_2(\rho-\rho')(|A_j|^4 \\ + 6|A_j|^2|A_{3-j}|^2 + 3|A_{3-j}|^4)A_j\,d\rho' = 0, \quad j = 1,2.\end{aligned} \tag{3}$$

The model (3) refers to the evolution of pump-probe pulses in the MDNC media where we have incorporated the phenomenological generic model of the nonlocal response of nonlinearity. The response function $\int_{-\infty}^{\infty} R(\rho-\rho')$ shows the surrounding spatial region, range, or domain of a homogenous isotropic MDNC medium responding to the refractive index change due to the intense pump pulse intensity at a point $\rho'$ in the medium. We take the intensity profile $I(\rho')$ and the width of the nonlocal response function $R(\rho-\rho')$ as comparable, owing to the general nonlocal nonlinear response. The cause of the nonlocal nonlinear response in the composite can be due to the phenomenon of advection or the thermal nonlinearity due to the presence of metal nanoparticles as described by Souza *et al.* [6]. The nonlinear response of the composite medium is given by various nonlocal response functions. Here we study the influence of various response functions on MI for different cases of nonlocal nonlinearities. The functions can be conveniently put into two classes based on whether the spectrum corresponding to the function is positive definite or not. The exponential and Gaussian functions belong to a positive definite spectrum, while rectangular and sine-oscillatory are not characterized by positive definite spectrum. For detailed study of the MI phenomenon, we specifically use the Gaussian and the rectangular response functions as the two representative categories. The various response functions and their Fourier transforms are tabulated in Table I and graphically represented as a function of the $\kappa$ vector in Fig. 1.

TABLE I. Various nonlocal response functions and their Fourier transforms.

| Function | $R(\rho)$ | $\hat{R}(\kappa)$ |
|---|---|---|
| Exponential | $\frac{1}{2\sigma}\exp(\frac{-\lvert\rho\rvert}{\sigma})$ | $\frac{1}{1+\sigma^2\kappa^2}$ |
| Gaussian | $\frac{1}{\sigma\sqrt{\pi}}\exp(\frac{-\rho^2}{\sigma^2})$ | $\exp(\frac{-\sigma^2\kappa^2}{4})$ |
| Rectangular | $\begin{cases}\frac{1}{2\sigma} & -\sigma \leqslant \rho \leqslant \sigma \\ 0 & \text{otherwise}\end{cases}$ | $\frac{\sin(\kappa\sigma)}{\kappa\sigma}$ |
| Sine-oscillatory | $\frac{1}{2\sigma}\sin(\frac{-\lvert\rho\rvert}{\sigma})$ | $\frac{1}{1-\sigma^2\kappa^2}$ |

## III. LINEAR STABILITY ANALYSIS

The stability of the steady-state solution against small perturbation for the propagation equation is studied using linear stability analysis. To be more realistic, we assume the asymmetric plane wave solutions whose intensity of

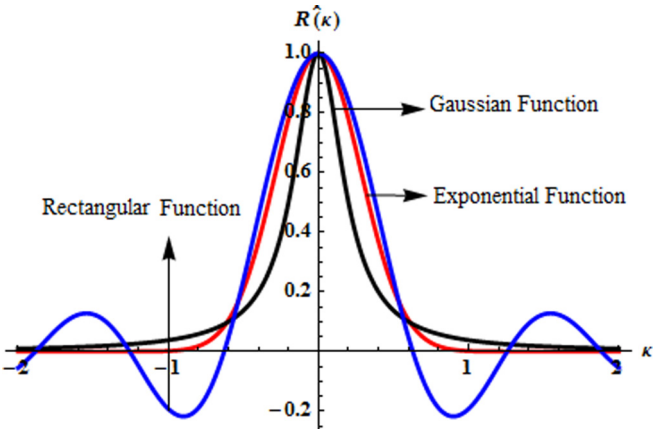


FIG. 1. Various response functions in the $\kappa$ space.

probe-pump beams is in the ratio 1:10 with a pump power of 31 kW and probe beam power of 3.1 kW [42]. The steady-state solution of Eq. (3) is given by

$$A_j(\rho,\xi) = \sqrt{P_j}\exp(i\,\phi_j\,\xi), \qquad j = 1,2, \tag{4}$$

where $P_j$ is the normalized pump and probe beam powers for $j = 1,2$. Perturbing the plane wave solution in its amplitude with the complex perturbations and further linearizing, we get the model equation in terms of the perturbations $a_j(\rho,\xi)$ and $a_{3-j}(\rho,\xi)$ as

$$\begin{aligned}
&\int_{-\infty}^{\infty}\sqrt{P_j}[2a_{3-j}(\rho',\xi)\sqrt{P_{3-j}}[r_1\alpha_1 + 3(P_j + P_{3-j})r_2\alpha_2] \\
&\quad + a_j(\rho',\xi)\sqrt{P_j}[r_1\alpha_1 + 2(P_j + 3P_{3-j})r_2\alpha_2] \\
&\quad + \sqrt{P_j}[r_1\alpha_1 + 2(P_j + 3P_{3-j})r_2\alpha_2]a_j^*(\rho',\xi) \\
&\quad + 2\sqrt{P_{3-j}}[r_1\alpha_1 + 3(P_j + P_{3-j})r_2\alpha_2]a_{3-j}^*(\rho',\xi)]\,d\rho' \\
&\quad + \frac{1}{2}\frac{\partial^2 a_j(\rho,\xi)}{\partial\rho^2} + (-1)^j i\frac{\partial a_j(\rho,\xi)}{\partial\xi} = 0,
\end{aligned} \tag{5}$$

where $r_1 = R_1(\rho - \rho')$ and $r_2 = R_2(\rho - \rho')$. We assume the following form of perturbation:

$$a_j(\rho,\xi) = a_{j1}(\rho,\xi) + i\,a_{j2}(\rho,\xi), \quad j = 1,2, \tag{6}$$

where $a_{j1}(\rho,\xi)$ and $a_{j2}(\rho,\xi)$ are the real and the imaginary parts of the perturbation with $a_j^*(\rho,\xi)$ as its complex conjugate. Substituting Eq. (6) into Eq. (5) and separating the real and imaginary parts from the linearized equation, we get

$$\begin{aligned}
&\frac{\partial a_{j1}(\rho,\xi)}{\partial\xi} + \frac{(-1)^j}{2}\frac{\partial^2 a_{j2}(\rho,\xi)}{\partial\rho^2} = 0, \\
&\int_{-\infty}^{\infty}\{[2P_j r_1\alpha_1 + 2(P_j + 3P_{3-j})r_2\alpha_2]a_{j1}(\rho',\xi) \\
&\quad + 4\sqrt{P_j}\sqrt{P_{3-j}}[r_1\alpha_1 + 3(P_j + P_{3-j})r_2\alpha_2]a_{(3-j)1}(\rho',\xi)\}\,d\rho' \\
&\quad + (-1)^{j+1}\frac{\partial a_{j2}(\rho,\xi)}{\partial\xi} + \frac{1}{2}\frac{\partial^2 a_{j1}(\rho,\xi)}{\partial\rho^2} = 0, \quad j = 1,2.
\end{aligned} \tag{7}$$

We apply the convolution theorem and use the Fourier transform [36] of the following form:

$$\begin{aligned}
\hat{a}_j(\kappa,\xi) &= \int_{-\infty}^{\infty} a_j(\rho,\xi)e^{i\kappa\rho}\,d\rho, \\
\hat{R}(\kappa) &= \int_{-\infty}^{\infty} R(\rho)e^{i\kappa\rho}\,d\rho.
\end{aligned} \tag{8}$$

We have the set of four differential equations as follows:

$$\begin{aligned}
&\frac{\partial\hat{a}_{j1}}{\partial\xi} + (-1)^j\frac{(i\kappa)^2}{2}\frac{\partial\hat{a}_{j2}}{\partial\rho^2} = 0, \\
&2P_1[\hat{R}_1\alpha_1 + 2(P_j + 3P_{3-j})\hat{R}_2\alpha_2]\hat{a}_{j1} \\
&\quad + 4\sqrt{P_j}\sqrt{P_{j-1}}\big[\hat{R}_1\alpha_1 + 3(P_j + P_{3-j})\hat{R}_2\alpha_2\big]\hat{a}_{(3-j)1} \\
&\quad + (-1)^{j+1}\frac{\partial\hat{a}_{j2}(\rho,\xi)}{\partial\xi} + \frac{(i\kappa)^2}{2}\frac{\partial^2\hat{a}_{j1}}{\partial\rho^2} = 0, \quad j = 1,2.
\end{aligned} \tag{9}$$

The coefficient matrix of the above equation can be obtained as

$$\begin{pmatrix} \mathbf{0} & -\frac{\kappa^2}{2} & \mathbf{0} & \mathbf{0} \\ \mathbf{m_1} & \mathbf{0} & -\mathbf{m_2} & \mathbf{0} \\ \mathbf{0} & \mathbf{0} & \mathbf{0} & \frac{\kappa^2}{2} \\ \mathbf{m_2} & \mathbf{0} & \mathbf{m_3} & \mathbf{0} \end{pmatrix}$$

where

$$\begin{aligned}
\mathbf{m_1} &= \tfrac{1}{2}[\kappa^2 - 4P_1\hat{R}_1\alpha_1 - 8P_1(P_1 + 3P_2)\hat{R}_2\alpha_2], \\
\mathbf{m_2} &= 4\sqrt{P_1}\sqrt{P_2}[\hat{R}_1\alpha_1 + 3(P_1 + P_2)\hat{R}_2\alpha_2], \\
\mathbf{m_3} &= \tfrac{1}{2}[-\kappa^2 + 4P_2\hat{R}_1\alpha_1 + 8P_2(3P_1 + P_2)\hat{R}_2\alpha_2].
\end{aligned}$$

We consider $\lambda$ as the eigenvalue of the above matrix, and one can write the characteristic equation of the above matrix as

$$|A - \lambda I| = 0. \tag{10}$$

Hence the eigenvalue $\lambda$ [36] of the coefficient matrix is given by

$$\lambda = \pm\tfrac{1}{2}\sqrt{\lambda_a \pm \lambda_b}, \tag{11}$$

where

$$\begin{aligned}
\lambda_a = \big[&-\kappa^4 + 2\kappa^2 P_2\hat{R}_1\alpha_1 + 4\kappa^2 P_1^2\hat{R}_2\alpha_2 + 4\kappa^2 P_2^2\hat{R}_2\alpha_2 \\
&+ 2\kappa^2 P_1(\hat{R}_1\alpha_1 + 12P_2\hat{R}_2\alpha_2)\big]
\end{aligned} \tag{12}$$

and

$$\begin{aligned}
\lambda_b = 2\kappa^2\sqrt{\big[}&4P_1^4\hat{R}_2^2\alpha_2^2 + P_2^2(\hat{R}_1\alpha_1 + 2P_2\hat{R}_2\alpha_2)^2 \\
&+ 4P_1^3\hat{R}_2\alpha_2(\hat{R}_1\alpha_1 + 36P_2\hat{R}_2\alpha_2) + 2P_1P_2\big(7\hat{R}_1^2\alpha_1^2 \\
&+ 46P_2\hat{R}_1\hat{R}_2\alpha_1\alpha_2 + 72P_2^2\hat{R}_2^2\alpha_2^2\big) + P_1^2\big(\hat{R}_1^2\alpha_1^2 \\
&+ 92P_2\hat{R}_1\hat{R}_2\alpha_1\alpha_2 + 280P_2^2\hat{R}_2^2\alpha_2^2\big)\big].
\end{aligned} \tag{13}$$

Hence $\lambda$ has four different values. The MI gain is given by

$$G(\kappa) = \mathrm{Re}\,\lambda. \tag{14}$$

We note that MI is possible only for the eigenvalue $\lambda = +\frac{1}{2}\sqrt{\lambda_a + \lambda_b}$ where both $\lambda_a$ and $\lambda_b$ are real for the condition $4\hat{R}_2^2\alpha_2^2(P_1^4 + P_2^4 + 36P_1^3P_2 + 36P_2^2 + 70P_1^2P_2^2) + \hat{R}_1^2\alpha_1^2(P_2^2 + 14P_1P_2 + P_1^2) > 4(P_2^2 + P_1^3 + 23P_1^2P_2)\hat{R}_1\hat{R}_2\alpha_1\alpha_2$. The spatial frequency corresponding to the maximum MI gain gives the optimum modulation frequency, which is given by

$$\frac{dG(\kappa)}{d\kappa} = 0. \tag{15}$$

## IV. MODULATIONAL INSTABILITY

As described earlier, one of the most sought features of the composite system is its ability to tailor the effective nonlinearity of the system, which can enable one to naively control the plasmonic effect of the system. By assuming a different combination of cubic and quintic nonlinearity in the nonlocal response regime, we study various features of MI. Along similar lines to the studies on MI, we first study the effect of power on MI due to nonlocal nonlinearity. Further keeping the cubic nonlinearity constant, we vary the coefficient of the

quintic nonlinearity and study the role of nonlocal responses on MI for various combinations of nonlinearities and strength of nonlocalities. We also consider an intriguing special case relevant to a composite system, where the cubic nonlinearity of the composite is null, while the effective nonlinearity can take finite values. For uniformity, we have used dotted lines to represent the rectangular response function and solid lines to represent the Gaussian response function.

### A. Effect of power

To start, it is customary to understand the influence of pump power on MI for different kinds of nonlinear response functions. We have considered three representative combinations of powers composing both symmetric and asymmetric solutions: (1) $P_1 = 1$, $P_2 = 0.1$ and (2) $P_1 = 4$, $P_2 = 0.4$ are the choice of powers for the asymmetric case, while (3) $P_1 = 1$, $P_2 = 1$ corresponds to the symmetric solution. We have plotted the Gaussian and the rectangular response functions separately with the nonlinear coefficients as $\alpha_1 = 1$ and $\alpha_2 = 0.1$ in Figs. 2(a) and 2(b), respectively. It is noted from Figs. 2(a) and 2(b) that MI gain increases with power for both response functions as expected. The rectangular response function showed an increase in the MI gain and number of bands with power. For a Gaussian response function, MI gain increases with power for all cases of nonlinearities. In Fig. 2(c), where we have considered the Gaussian response function with symmetric power and the strength of nonlinearities as $\alpha_1 = 1$ and $\alpha_2 = -0.1$ an anomaly noted is that here MI gain decreases for $P_1 = P_2 = 1$ to $P_1 = P_2 = 2$. At a power of 2 there is absolutely no MI, and a further increase in power increases the MI gain. Apart from this, the symmetric solution in particular doesn't have any distinguished effect on MI from the asymmetric solution. Hence for further discussion, we consider only the asymmetric solutions.

### B. Effect of nonlocal strength

As the nonlocality plays a crucial role in the dynamics of MI, in Fig. 3 we show the contour map of MI spectra as a function of nonlocal strength. A general behavior noticeable in the MI spectrum is that the nonlocal strength monotonously decreases both the gain and bandwidth of the MI bands [Figs. 3(a) and 3(b)]. Thus the nonlocal effect suppresses the MI. Interestingly, the rectangular response function shows additional sidebands at higher $\kappa$, whose gain shows an unusual increase with $\sigma$ as shown in Fig. 3(b). The MI features due to different nonlocal response will be highlighted and comprehensively analyzed at different settings of nonlinearity in the following sections.

### C. MI at different settings of nonlinear response

The study of MI in the HON regime is interesting as it could lead to many new features, which would otherwise be impossible in the conventional system with only cubic nonlinearity. For instance, the quintic nonlinearity can either enhance or suppress MI and at some parametric conditions can promote new sidebands. In what follows, we consider three different regimes of nonlinearity based on the sign of cubic nonlinearity and study MI with a particular emphasis on the nonlocal nonlinear response and quintic nonlinearity.

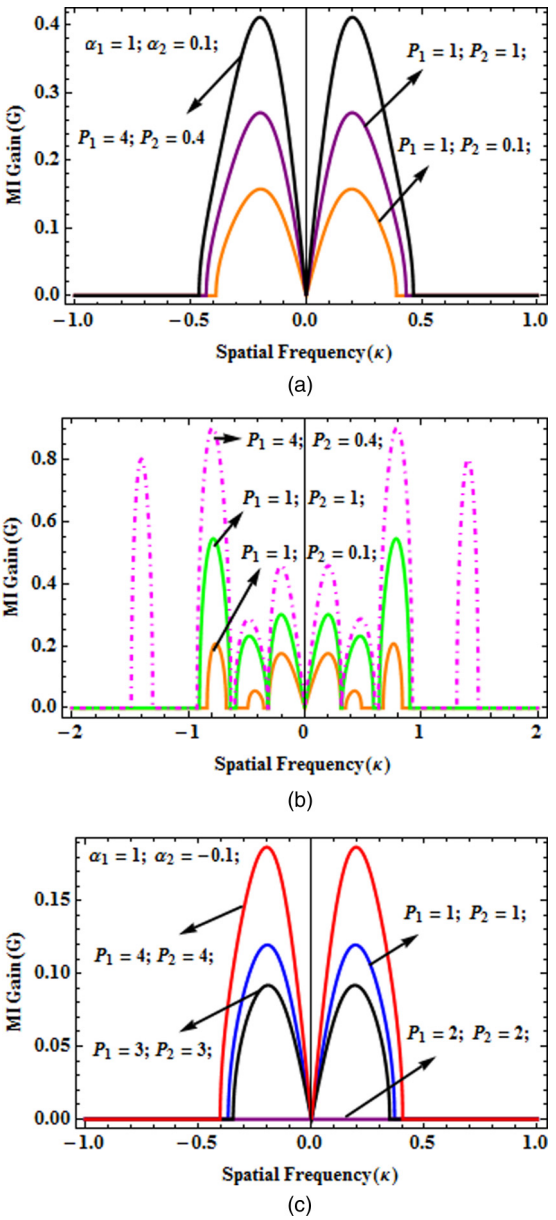


FIG. 2. The variation of MI gain spectra with power for the focusing nonlinearity with (a) Gaussian response function and (b) rectangular response function varying power as $P_1 = 1, P_2 = 0.1$, $P_1 = 1, P_2 = 1$, and $P_1 = 4, P_2 = 0.4$, and the strength of nonlocality is $\sigma = 10$ and the strength of nonlinearity as (a) $\alpha_1 = 1, \alpha_2 = 0.1$, (b) $\alpha_1 = 1, \alpha_2 = 0.1$, (c) $\alpha_1 = 1, \alpha_2 = -0.1$, and the power varying symmetrically as $P_1 = P_2 = 1, 2, 3$, and 4 for the Gaussian response function.

#### *1. Focusing nonlinearity ($\alpha_1 > 0$)*

This is a typical case of spatial MI, where MI is generally possible owing to the phase matching between the positive nonlinearity and diffraction. Two distinct types of nonlocal response, namely, Gaussian and rectangular response function, have been considered, and the MI is studied for different combinations of cubic and quintic nonlinearities as portrayed in Fig. 4. With proper understanding of the effect of nonlocal strength from the previous section, to highlight other interesting features due to interplay between HON and nonlocality, we

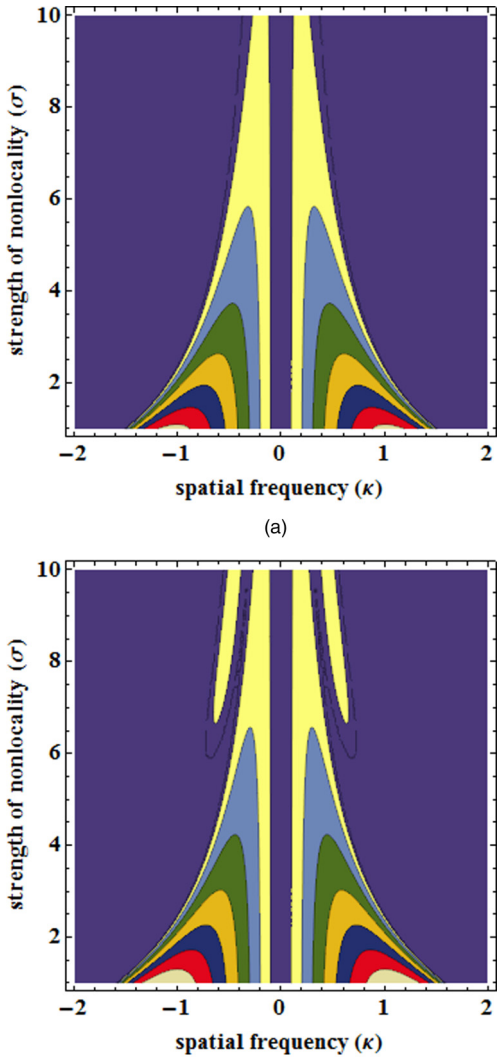


FIG. 3. The MI gain spectra as a function of strength of nonlocality for (a) the Gaussian response and (b) rectangular response for $P_1 = 1$, $P_2 = 1$ and $\alpha_1 = 1, \alpha_2 = -0.1$.

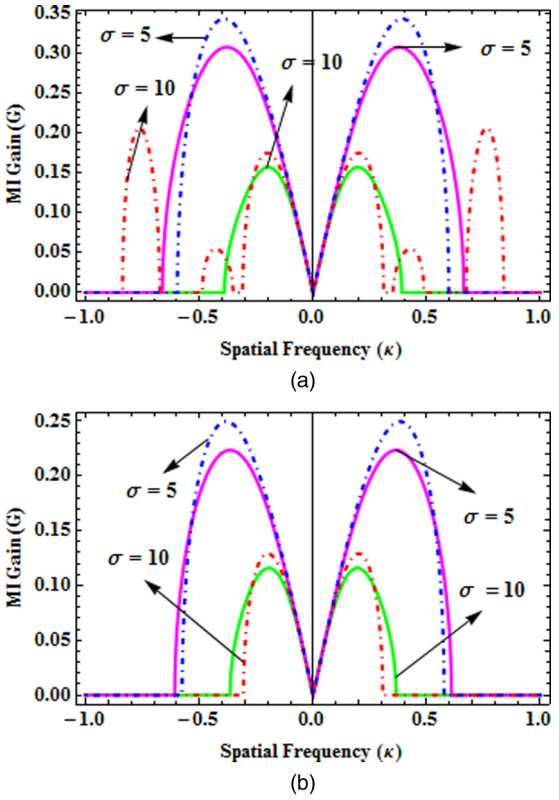


FIG. 4. The MI gain spectra for the focusing nonlinearity with different nonlocal response function and varying the strength of nonlocality as $\sigma = 5, 10$ and the strength of nonlinearity as (a) $\alpha_1 = 1, \alpha_2 = 0.1$, (b) $\alpha_1 = 1, \alpha_2 = -0.1$ with other parameters as $P_1 = 1$ and $P_2 = 0.1$.

choose two representative values of $\sigma = 5$ and 10. Figure 4(a) represents the case of $\alpha_1 > 0$ and $\alpha_2 > 0$, where both nonlinear effects constructively reinforce to cause MI through phase matching with diffraction effects, as in the case of conventional scalar MI. This case is characterized by higher gain due to the enhancement of the effective nonlinearity as a result of the accumulated nonlinearity due to cubic and quintic effects. The rectangular function behaves qualitatively different leading to the emergence of new spectral sidebands which we refer to as secondary bands, while the Gaussian response behaves quite similarly to conventional MI. Figure 4(b) corresponds to the case of $\alpha_1 > 0$ and $\alpha_2 < 0$, where both nonlinear effects compete due to the opposite sign, and the resulting instability spectrum shows MI bands with reduced gain, regardless of the nature of nonlocality. In this case, both the Gaussian (solid line) and rectangular functions behave quite close, except the fact that the gain of primary band of the rectangular function is more than, and conversely the bandwidth is lesser than, the Gaussian function. It is also apparent from Fig. 4 that the increase in the strength of the nonlocality decreases the gain of MI, and in particular, new spectral bands originate for higher values of $\sigma$.

#### *2. Zero cubic nonlinearity ($\alpha_1 = 0$)*

This is particularly an intriguing situation ($\alpha_1 = 0$ and $\alpha_2 \neq 0$) typically characteristic to the composite structures. Here, by proper choice of the volume fraction of the nanoparticles in the composite, one can delicately nullify the lower order nonlinear effects (cubic nonlinearity in the present setting), leaving only the next higher order effects to take control on the nonlinear effects of the system. Taking advantage of this unique feature, we consider a different combination of quintic nonlinearity based on its sign. Figure 5(a) represents the instability spectra for $\alpha_1 = 0$ and $\alpha_2 > 0$, where the much needed phase-matching condition for the MI process is satisfied by the positive (focusing) quintic nonlinearity, a process quite similar to the conventional MI with cubic nonlinearity. Figure 5(b) is the situation where the quintic nonlinearity takes negative value, but MI still is made possible due to XPM effects because of the destabilization of the steady state by XPM. It should be noted that, once the XPM effects are ignored, this particular case is implausible for MI. In both cases of quintic nonlinearity, the rectangular function dominates the gain, with additional sidebands for the case of $\alpha_2 < 0$. The effect of nonlocal strength in this case is rather interesting, such that the secondary spectral bands register a higher gain

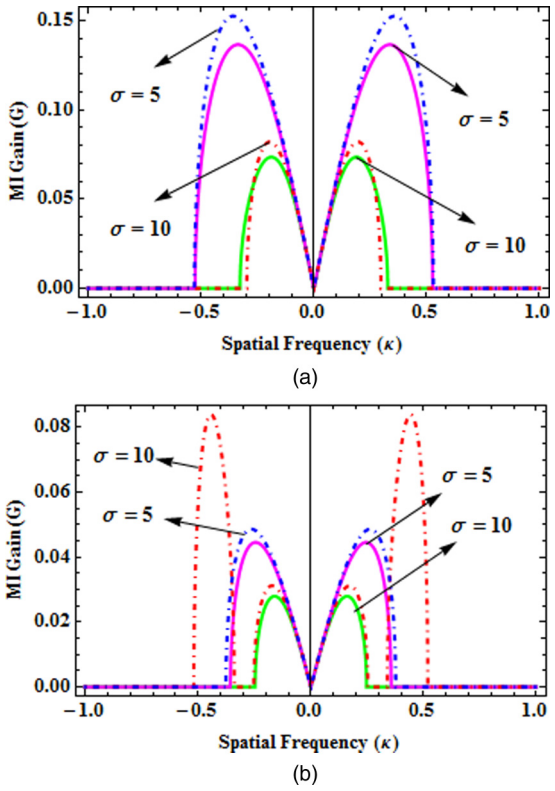


FIG. 5. The MI gain spectra for the absence of cubic nonlinearity with varying the strength of nonlocality as $\sigma = 5,10$ and the strength of nonlinearity as (a) $\alpha_1 = 0, \alpha_2 = 0.1$, (b) $\alpha_1 = 0, \alpha_2 = -0.1$ with the other parameters as $P_1 = 1$ and $P_2 = 0.1$.

whose peak gain is more than twice the gain of the primary band. This is attributed to the fact that the quintic nonlinearity generally promotes higher order spectral bands, and with an increase in the strength of the nonlocality, both collectively act to enhance the gain. As this case is particularly dominated by quintic nonlinearity, it is interesting to understand the strength of quintic nonlinearity in the MI spectrum. Figure 6 shows the evolution of spectral bands with strength of quintic nonlinearity for both cases of nonlocal functions. In both cases, $|\alpha_2|$ enhance MI by increasing the gain of MI as well as the number of sidebands. In particular, the effect of $\alpha_2$ is more pronounced in a rectangular function with additional spectral bands of higher gain [Fig. 6(a)], while the Gaussian function behaves rather in a straightforward way, indicating a monotonous increase of gain with $\alpha_2$ as shown in Fig. 6(b).

### *3. Defocusing nonlinearity ($\alpha_1 < 0$)*

The defocusing nonlinearity is characterized by the negative values of the cubic nonlinearity, and therefore, the MI can be realized either by virtue of quintic nonlinearity or through the XPM effects. Like in the previous section, two different combinations of cubic and quintic nonlinearities given by different signs of $\alpha_2$ are considered. Figure 7(a) represents the MI spectra corresponding to $\alpha_1 < 0$ and $\alpha_2 > 0$. In this case MI is possible by means of the focusing quintic nonlinearity and crucially depends on the relative strength of $\alpha_1$ and $\alpha_2$, as both are in the opposite sign. One interesting feature of this

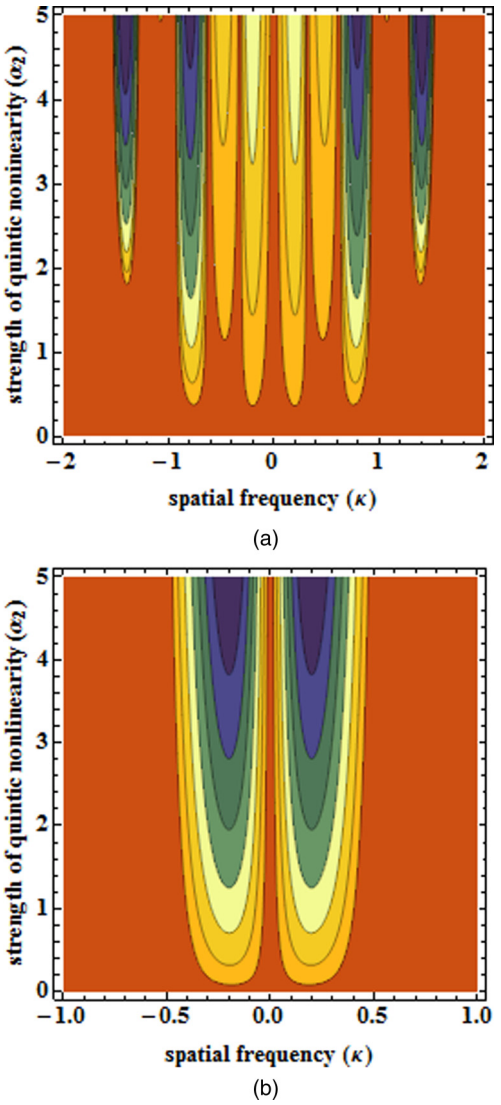


FIG. 6. The MI gain spectra for the varying strength of quintic nonlinearity for the (a) rectangular and (b) Gaussian response functions with the other parameters as $\sigma = 10$, $\alpha_1 = 0$ $P_1 = 1$, and $P_2 = 0.1$.

particular case is the emergence of the additional sidebands even for a lower value of $\sigma$ for the rectangular response function. This emphasizes the relevance of the quintic nonlinearity in the promotion of additional sidebands. Also, the relative secondary to primary peak gain is higher than the previous case of zero cubic nonlinearity. This quite clearly establishes the constructive interplay between quintic nonlinearity and the nonlocal strength in the emergence of higher order sidebands. The Gaussian response shows a monotonous variation with strength of nonlocality as predicted in other cases. However, the registered MI gain is lower than the focusing cubic nonlinearity, which is clearly due to the weakened quintic nonlinearity of choice in this present case.

Figure 7(b) is the case of $\alpha_1 < 0$ and $\alpha_2 < 0$ where both nonlinearities are defocusing and the MI is realized purely by means of XPM effects and when the cross coupling effects are turned off, and there is no instability in the case. So XPM

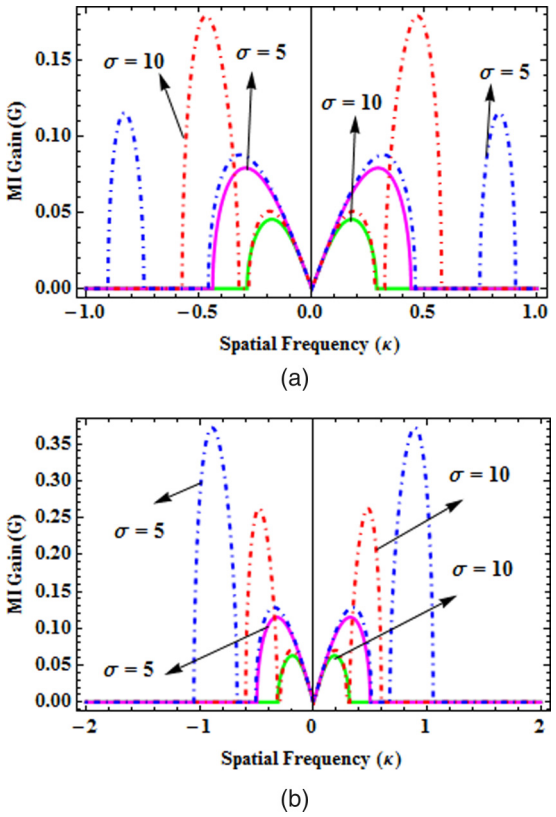


FIG. 7. The MI gain spectra for the defocusing nonlinearity with different nonlocal response function and varying the strength of nonlocality as $\sigma = 5,10$ and the strength of nonlinearity as (a) $\alpha_1 = -1, \alpha_2 = 0.1$, (b) $\alpha_1 = -1, \alpha_2 = -0.1$, and $P_1 = 1$, $P_2 = 0.1$.

plays a critical role in the origin of MI in this regime. In this case, the nonlinearities only enhance the gain and are not fundamental to the existence of instability. As in the previous case, the nonlocal strength decreases the MI gain, but for the choice of the parameters no higher order sidebands are noticed.

### D. Results and discussions

For a comprehensive picture and to make the discussion self-explanatory, we reproduce some of the results corresponding to the scalar spatial MI [38,39] and compare with the present results on a counterpropagating coupled system. Figure 8 shows the MI spectra for three different cases of cubic nonlinearity as discussed above. As the spectrum is symmetric $G(-\kappa) = G(\kappa)$, we are content to show only the positive spectrum. To facilitate comparison with the previous discussion of the counterpropagating case, we ideally choose the same configuration of signs of $\alpha_1$ and $\alpha_2$ as before. Figure 8(a) shows the MI of the focusing cubic media, where the solid line represents the Gaussian response, while the dashed line is the case of a rectangular nonlocal response. Two choices of quintic nonlinearity have been considered depending on the sign of $\alpha_2$. Figure 8(a) corresponds to the conventional MI, which has been studied extensively, and an indepth discussion is needless here. It is apparent that the MI gain is significantly lower than the gain corresponding to Fig. 4, which agrees with the results reported in the MI with local nonlinear response [41]. The case of zero cubic nonlinearity shown in Fig. 8(b) clearly shows the absence of MI when $\alpha_2 < 0$, which is due to the lack of phase matching between diffraction and a defocusing nonlinear effect. However, for the present problem on counterpropagation case as shown by Fig. 5, MI has been realized regardless of the sign of the quintic nonlinearity. The last is the case of defocusing cubic nonlinearity: in this case the origin of MI critically depends on the relative strength of $\alpha_1$ and $\alpha_2$. Defocusing quintic nonlinearity [Fig. 8(c)] is generally not feasible for MI; however, for the case of a rectangular nonlocal function, a secondary spectral band at higher $\kappa$ is noted, while the Gaussian function is not unstable and no MI is noticed. This observation is different from Fig. 7 for a coupled system, where regardless of the combination of signs $\alpha_1$ and $\alpha_2$ the instabilities are inevitably noticed.

For better insight and to give a global picture of the effect of various forms of popular nonlocal responses in the MI of a composite system, we plot in Fig. 9 the MI spectrum for different forms of available nonlocal functions. As discussed earlier, the various nonlocal functions are broadly classified into two classes, namely, a definite and indefinite positive spectrum. So far, our whole study has been based on a representative case of nonlocal functions from each category, namely, Gaussian and rectangular functions. It is quite evident that both classes of nonlocal functions behave qualitatively different, which is also evident from Fig. 9.

The solid curve corresponds to exponential and Gaussian responses belonging to a positive definite spectrum, where the behavior of MI bands is similar to the local nonlinear system, the difference being the magnitude of MI gain as a result of the change in the effective nonlinearity. However, the nonlocal response without a positive definite spectrum such as rectangular and sine-oscillatory is in fact interesting for MI,

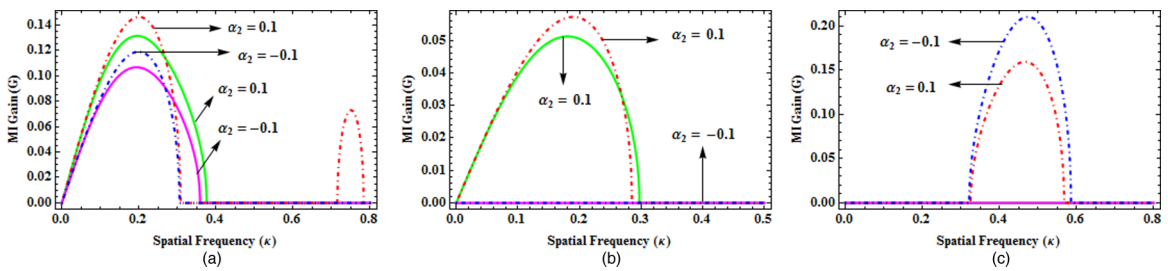


FIG. 8. The MI gain spectra for the scalar NLS equation with the strength of nonlinearity as (a) $\alpha_1 = 1$, (b) $\alpha_1 = 0$, (c) $\alpha_1 = -1$ and with the other parameters as $P_1 = 1$, $P_2 = 0$, $\sigma = 10$, and $\alpha_2$ having values 0.1 and $-0.1$ in each case.

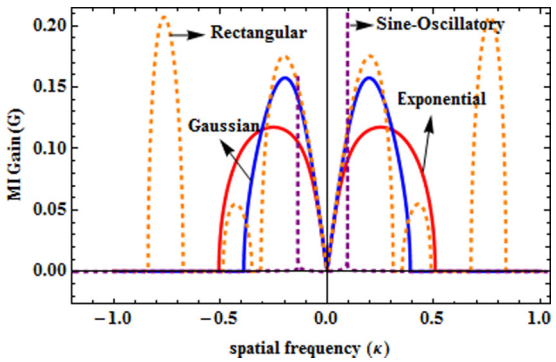


FIG. 9. The MI gain spectra for different nonlocal response function with the various parameters as $\sigma = 10$, $\alpha_1 = 1$,$\alpha_2 = 0.1$, $P_1 = 1$, and $P_2 = 0.1$.

as it would lead to increased gain and an additional instability window at higher $\kappa$ as represented by dashed lines in Fig. 9. The strength of nonlinearity also plays an important role, especially for the case of a rectangular function, as a new spectral band originates, which is found to be sensitive to $\sigma$ (refer to Fig. 9).

Moreover, it should be noted that in addition to the nonlocality, the relative strength of the nonlinearity ($\alpha_1/\alpha_2$) and the cross coupling effects are decisive in the origin and the control of MI dynamics. For instance, there are cases like zero cubic and defocusing quintic nonlinearity [Fig. 5(b)] and defocusing cubic and quinitic [Fig. 7(b)], where the MI is attributed to the XPM effects, which destabilize the steady-state solution to cause MI [refer to Figs. 5(b) and 7(b)]. However, in the case of focusing quintic nonlinearity, regardless of the sign of cubic nonlinearity, the phase matching for MI is satisfied through focussing quintic nonlinearity [Figs. 5(a) and 7(a)]. Apart from XPM effects, the relative strength of nonlinearity plays a substantial role in the emergence of additional sidebands in MI, which is particularly true for rectangular functions. It is noticed that depending on the value of the relative strength of nonlinearity, more additional bands are observed. Interestingly, for a zero cubic and defocusing cubic, for the parameter of choice, the MI gain of the secondary bands dominates, whose gain is nearly double than the conventional band.

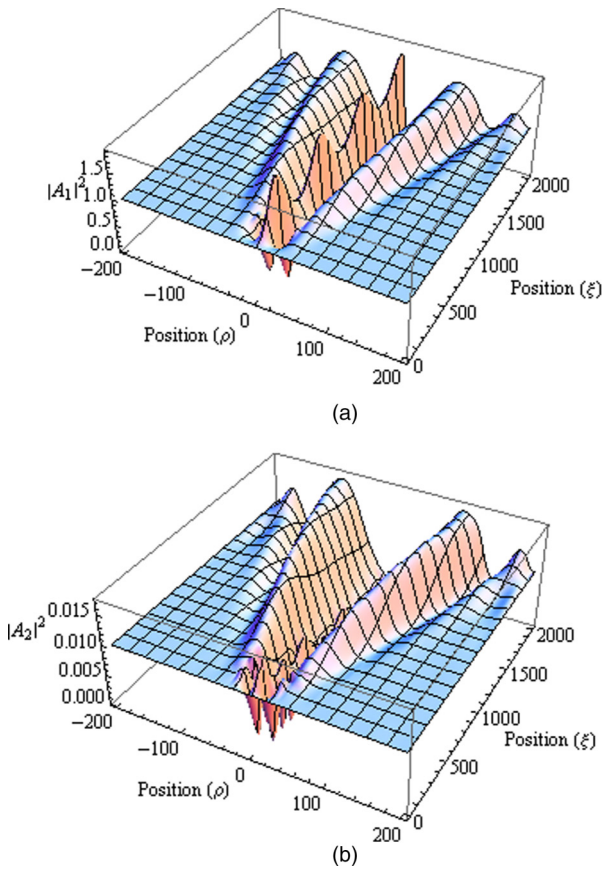


FIG. 10. The direct simulation of the evolution of the (a) pump and the (b) probe beams with the the nonlocal response function as the Gaussian function and the other parameters as $\alpha_1 = 0$, $\alpha_2 = 0.1$, $\sigma = 10$, $A_{10} = 1$, $A_{20} = 0.1$, and $\omega_0 = 0.5$.

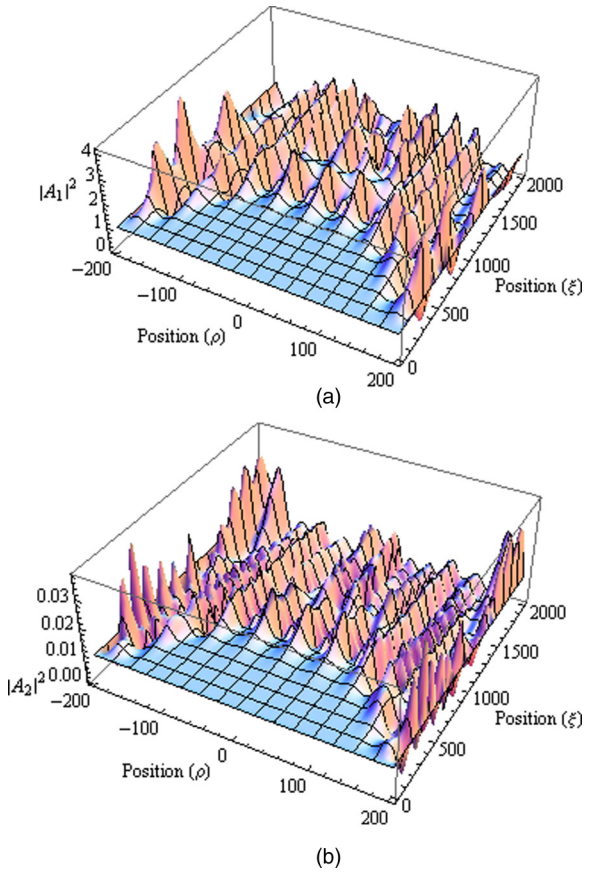


FIG. 11. The direct simulation of the evolution of the (a) pump and the (b) probe beams with the the nonlocal response function as the rectangular function and the other parameters as $\alpha_1 = 0$,$\alpha_2 = 0.1$, $\sigma = 10$, $A_{10} = 1$, $A_{20} = 0.1$, and $\omega_0 = 0.5$.

For numerical appreciation, we numerically simulate Eq. (3) and we choose the perturbed solution as $A_1 = A_2 = A_{j0} + a_0 Cos(\omega_0 \rho)$, where $A_{j0}$ is the amplitude of the propagating pump-probe beams, $a_0 = 10^{-4}$ is the small perturbation in the amplitude, and $\omega_0$ is the optimum modulation frequency. $\xi = 2000$ is the dimensionless length of beam propagation, such that $z = \xi K^{-1}$ gives 0.121 cm as the length in units and $\rho$ is the dimensionless transverse direction in the range $-200$ to 200. We consider the strength of nonlocality as $\sigma = 10$. Figures 10 and 11 show the qualitative results of the numerical

simulation showing the instability as the wave propagates along the $z$ direction.

## V. CONCLUSION

We have theoretically studied the modulational instability of a composite system showing a nonlocal nonlinear response. For our purposes, we have chosen the recent experimentally realized composite system of silver nanoparticels in acetone. Such a system enables one to realize a desired nonlinearity by properly choosing the volume fraction of the nanoparticles in the composite. This striking feature of such a system is particularly attractive for nonlinear management. Taking advantage of this feature we have assumed different combinations of signs of nonlinearity, and we systematically studied the dynamics of MI with particular emphasis on nonlocal nonlinearity. To generalize the impact of nonlocality, the commonly available form of nonlocal response functions has been considered. It is quite obvious from our study that the nonlocal response decreases the gain and bandwidth of MI, while at a particular combination of the quintic nonlinearity it can even promote new spectral bands. The rectangular response function is particularly attractive in MI dynamics, as it enables additional instability windows, whose width and numbers crucially depend on the strength of nonlocality. As far as cross coupling effects are concerned, the MI is typically enhanced by XPM, and especially in the defocusing nonlinearity, the XPM effects are found to be fundamental to the origin of MI. The relative strength of nonlinearity is another factor playing a substantial role either by increasing the gain or by promoting new spectral bands. We also noticed that the choice of the nonlocal response is indeed crucial, and the interplay with the nonlinearity accordingly impacts the MI dynamics. Thus we comprehensively studied the MI dynamics in the composite system with competing nonlinearities with a particular emphasis on the nonlocal nonlinear response. As there are few works on the fabrication of composite systems, we believe our theoretical results could simulate new experiments, especially in the context of nonlinear plasmonics.

## ACKNOWLEDGMENTS

K.P. thanks the agencies Department of science and technology-Science and Engineering Research Board (DST-SERB), Council of Scientific and Industrial Research (CSIR), National Board of Higher Mathematics (NBHM), Indo-French Centre for the promotion of Advanced Research (IFCPAR/CEFIPRA) and Department of Science and Technology-Foundation for Science and Technology (DST-FCT), funded by the Government of India, for financial support through major projects. K.N. acknowledges Centre national de la recherche scientifique (CNRS) for support through a post-doctoral fellowship at the Université de Bourgogne, Dijon, France, and the Agence Nationale de la Recherche (ANR) for support through the research fellowship at the Université de Grenoble-Alpes, Grenoble, France.

[1] N. Lepeshkin, W. Kim, V. Safonov, J. Zhu, R. Armstrong, C. White, R. Zuhr, and V. Shalaev, J. Nonlinear Opt. Phys. Mater. **8**, 191 (1999).
[2] X. Jiang, K. Guo, G. Liu, T. Yang, and Y. Yang, Superlattices Microstruct. **105**, 56 (2017).
[3] Y. Tsutsui, T. Hayakawa, G. Kawamura, and M. Nogami, Nanotechnology **22**, 275203 (2011).
[4] P. P. Kiran, B. N. S. Bhaktha, D. N. Rao, and G. De, J. Appl. Phys. **96**, 6717 (2004).
[5] Y. X. Zhang and Y. H. Wang, RSC Adv. **7**, 45129 (2017).
[6] R. Souza, M. Alencar, E. Da Silva, M. Meneghetti, and J. Hickmann, Appl. Phys. Lett. **92**, 201902 (2008).
[7] A. Stalmashonak, G. Seifert, and A. Abdolvand, in *Optical Properties of Nanocomposites Containing Metal Nanoparticles*, edited by A. Stalmashonak, G. Seifert, and A. Abdolvand (Springer, Heidelberg, 2013), pp. 5–15.
[8] M. Kauranen and A. V. Zayats, Nat. Photon. **6**, 737 (2012).
[9] A. S. Reyna, K. C. Jorge, and C. B. de Araújo, Phys. Rev. A **90**, 063835 (2014).
[10] A. Griesmaier, J. Stuhler, T. Koch, M. Fattori, T. Pfau, and S. Giovanazzi, Phys. Rev. Lett. **97**, 250402 (2006).
[11] M. Warenghem, J. F. Blach, and J. F. Henninot, J. Opt. Soc. Am. B **25**, 1882 (2008).
[12] V. M. Pérez-García, V. V. Konotop, and J. J. García-Ripoll, Phys. Rev. E **62**, 4300 (2000).
[13] J. F. Corney and O. Bang, Phys. Rev. E **64**, 047601 (2001).
[14] S. Skupin, M. Saffman, and W. Królikowski, Phys. Rev. Lett. **98**, 263902 (2007).
[15] Y.-L. Zhou, Z.-L. Zou, and K. Yan, Water Sci. Eng. **5**, 419 (2012).
[16] M. Brunetti and J. Kasparian, Phys. Lett. A **378**, 3626 (2014).
[17] G. Murtaza and M. Salahuddin, Plasma Phys. **24**, 451 (1982).
[18] O. Bouzit, M. Tribeche, and A. Bains, Phys. Plasmas **22**, 084506 (2015).
[19] G. Agrawal, *Nonlinear Fiber Optics* (Academic Press, Singapore, 2013).
[20] V. V. Konotop and M. Salerno, Phys. Rev. A **65**, 021602(R) (2002).
[21] L. Li, Z. Li, B. A. Malomed, D. Mihalache, and W. M. Liu, Phys. Rev. A **72**, 033611 (2005).
[22] E. Wamba, A. Mohamadou, and T. Kofané, J. Phys. B **41**, 225403 (2008).
[23] M. Peccianti, C. Conti, G. Assanto, A. DeLuca, and C. Umeton, in *The 16th Annual Meeting of the IEEE Lasers and Electro-Optics Society, 2003, LEOS 2003* (IEEE, Piscataway, NJ, 2003), Vol. 1, pp. 31–32.
[24] T. P. Horikis, Phys. Lett. A **380**, 3473 (2016).
[25] J. Beeckman, X. Hutsebaut, M. Haelterman, and K. Neyts, Opt. Express **15**, 11185 (2007).
[26] R. E. Noskov, P. A. Belov, and Y. S. Kivshar, Phys. Rev. Lett. **108**, 093901 (2012).
[27] D. Korobko, S. Moiseev, and I. Zolotovskii, Opt. Lett. **40**, 4619 (2015).
[28] M. Kumar, K. Porsezian, P. Tchofo-Dinda, P. Grelu, T. Mithun, and T. Uthayakumar, J. Opt. Soc. Am. B **34**, 198 (2017).
[29] K. Nithyanandan, R. V. J. Raja, T. Uthayakumar, and K. Porsezian, in *2012 International Conference on Optical Engineering, ICOE 2012* (IEEE, Piscataway, NJ, 2012), pp. 1–6.
[30] M. Saha and A. K. Sarma, Opt. Commun. **291**, 321 (2013).

[31] M. Saffman, G. McCarthy, and W. Królikowski, J. Opt. B **6**, S397 (2004).
[32] E. O. Alves, W. B. Cardoso, and A. T. Avelar, J. Opt. Soc. Am. B **33**, 1134 (2016).
[33] W. Królikowski, O. Bang, N. I. Nikolov, D. Neshev, J. Wyller, J. J. Rasmussen, and D. Edmundson, J. Opt. B **6**, S288 (2004).
[34] E. V. Doktorov and M. A. Molchan, Proc. SPIE **6725**, 672513 (2007).
[35] A. S. Reyna and C. B. de Araújo, Phys. Rev. A **89**, 063803 (2014).
[36] W. Krolikowski, O. Bang, J. J. Rasmussen, and J. Wyller, Phys. Rev. E **64**, 016612 (2001).
[37] Z. Wang, Q. Guo, W. Hong, and W. Hu, Opt. Commun. **394**, 31 (2017).
[38] C. L. Tiofack, H. Tagwo, O. Dafounansou, A. Mohamadou, and T. Kofane, Opt. Commun. **357**, 7 (2015).
[39] H. Tagwo, C. Tiofack, O. Dafounansou, A. Mohamadou, and T. Kofane, J. Mod. Opt. **63**, 558 (2016).
[40] G. P. Agrawal, Phys. Rev. Lett. **59**, 880 (1987).
[41] K. Nithyanandan, R. V. J. Raja, K. Porsezian, and B. Kalithasan, Phys. Rev. A **86**, 023827 (2012).
[42] A. S. Reyna and C. B. de Araújo, Opt. Express **22**, 22456 (2014).
[43] B. K. Esbensen, A. Wlotzka, M. Bache, O. Bang, and W. Krolikowski, Phys. Rev. A **84**, 053854 (2011).
[44] J. Wyller, W. Krolikowski, O. Bang, and J. J. Rasmussen, Phys. Rev. E **66**, 066615 (2002).
[45] Q. Kong, Q. Wang, O. Bang, and W. Krolikowski, Opt. Lett. **35**, 2152 (2010).